Journal of Power Sources 195 (2010) 4002–4012

Contents lists available at ScienceDirect

Journal of Power Sources

journal homepage: www.elsevier.com/locate/jpowsour

Direct utilization of methanol on impregnated Ni/YSZ and Ni–$Zr_{0.35}Ce_{0.65}O_2$/YSZ anodes for solid oxide fuel cells

Massimiliano Cimenti, Vanesa Alzate-Restrepo, Josephine M. Hill*

Department of Chemical and Petroleum Engineering, Schulich School of Engineering, University of Calgary, 2500 University Dr. NW, Calgary, AB T2N 1N4, Canada

ARTICLE INFO

Article history:
Received 27 October 2009
Received in revised form
23 December 2009
Accepted 29 December 2009
Available online 14 January 2010

Keywords:
Solid oxide fuel cells
Direct utilization
Methanol
Carbon formation
Ni/YSZ
Ni/$Zr_{0.35}Ce_{0.65}O_{2-\delta}$

ABSTRACT

Some of the limits on fuel cell development include the issues of hydrogen availability and storage. Methanol has many advantages as an alternative fuel for fuel cells but depending on the anode composition, the formation of carbon may be a problem. In this paper, the direct utilization of methanol in solid oxide fuel cells with impregnated Ni/YSZ and Ni–$Zr_{0.35}Ce_{0.65}O_{2-\delta}$ (ZDC)/YSZ anodes was investigated at 1073 K. Performance and stability of these anodes, as measured by steady-state polarization and electrochemical impedance spectroscopy, were improved by the presence of ZDC; although, the deposition of carbon, as detected by scanning electron microscopy and temperature-programmed oxidation analysis, was not entirely avoided. The impact of the carbon, however, was different depending on the anode. That is, carbon formation caused the delamination of impregnated Ni/YSZ anodes, while the structural integrity of Ni–ZDC/YSZ anodes was maintained and the cell performance was not negatively impacted. Increasing the fuel utilization decreased coking, as predicted by equilibrium calculations.

1. Introduction

Solid oxide fuel cells (SOFCs) are electrochemical devices for the simultaneous generation of electrical power and heat, and are characterized by high efficiency and low direct emissions [1]. Recently there has been interest in developing SOFC for small auxiliary power units (<10 kW) and portable power generation [2], in which case it would be convenient to operate the fuel cells directly with liquid fuels, such as alcohols, rather than with hydrogen (H_2). Methanol (MeOH) could be a convenient fuel [3] because no pre-treatment is required given the low level of impurities in commercial-grade MeOH [4], and the risk of severe coking is less compared to other liquid hydrocarbons [5].

Presently there are only a few publications on the direct utilization of MeOH with nickel/yttria-stabilized zirconia (Ni/YSZ) anodes [6,7]. Jiang and Virkar [6] tested anode-supported Ni/YSZ cells with pure MeOH and obtained maximum power densities of 1.3 and 0.6 W cm^{-2} at 1073 and 923 K, respectively. At the end of these tests, no carbon was visible, but no results on the long-term stability or information on the testing protocols (e.g., overall time of exposure to MeOH) were provided. These results demonstrate the feasibility of direct utilization of MeOH on Ni/YSZ anodes, but more testing is required to prove the long-term stability at low or zero fuel utilization, which are the most favorable conditions for coking.

Sasaki et al. [7] tested electrolyte-supported Ni/YSZ anodes with pure MeOH at 1273 K and the performance in MeOH was similar to the performance obtained with a mixture of H_2 and CO (molar ratio of 2:1). These results suggested that MeOH was completely decomposed by gas phase and surface reactions before reaching the electrochemically active layer in the anode. Again no coking was observed, in agreement with the thermodynamic predictions for 1273 K [8].

These results are consistent with thermodynamic calculations [8] that predict the propensity to form carbon decreases with increasing temperature when an SOFC is operated directly with MeOH. Carbon formation also decreases with increasing fuel utilization and the minimum fuel utilization for avoiding coking can be calculated for each operating temperature and pressure. At 1073 K and 1 atm, this minimum value is ~2% [8].

In practice, SOFC will be operated over a range of fuel utilizations including open circuit voltage (OCV) (i.e., zero fuel utilization). Exposure of Ni/YSZ to pure MeOH at OCV and 1073 K for more than 12 h did result in visible coking, and subsequent deformation and delamination of the electrode [9].

One strategy to avoid deactivation due to coking is the use of alternative anode materials. For the direct utilization of MeOH the alternative anodes tested include lanthanum cobaltite ($LaCoO_3$) [10], copper/gadolina-doped ceria (Cu/GDC) [11], and copper/ceria (Cu/CeO_2) [12]. Unfortunately, all of these materials were unstable.

* Corresponding author. Tel.: +1 403 210 9488; fax: +1 403 284 4852.
E-mail addresses: max.cimenti@afcc-auto.com (M. Cimenti), valzate.alzate@nrc-cnrc.gc.ca (V. Alzate-Restrepo), jhill@ucalgary.ca (J.M. Hill).

0378-7753/$ – see front matter © 2010 Elsevier B.V. All rights reserved.
doi:10.1016/j.jpowsour.2009.12.119

Nomenclature

APD	average performance decay
ASR	area specific resistance
EDX	energy-dispersive X-ray analysis
EIS	electrochemical impedance spectroscopy
LSM	$La_{0.8}Sr_{0.2}MnO_{3-\delta}$ cathode
KKT	linear Kramers–Kronig transformation
MeOH	methanol
mGC	micro-gas chromatograph
MS	mass-spectrometer analyzer
Ni/YSZp	impregnated Ni/YSZ anode
Ni/ZDC	Ni–$Zr_{0.35}Ce_{0.65}O_2$ anode
OCV	open circuit voltage
SEM	scanning electron microscopy
SOFC	solid oxide fuel cells
STP	standard temperature and pressure
TPO	temperature programmed oxidation
YSZ	$Y_{0.08}Zr_{0.92}O_{2-\delta}$ electrolyte
ZDC	zirconia-doped ceria, $Zr_{0.35}Ce_{0.65}O_2$

For ceria-based anodes instability was attributed to Cu sintering and surface instability of ceria [12]. Thermal stability and compatibility of ceria with the electrolyte (YSZ) can be improved by doping ceria with zirconia ($Zr_xCe_{1-x}O_2$) [13]. Specifically, the presence of Zr^{4+} ions in the lattice improves both oxygen storage capacity and ionic conductivity of ceria [14], and also increases the adsorption capacity for H_2 and CO [15], which may increase the rate of electrochemical oxidation of these species. In fact, the rate of electrochemical oxidation of H_2 and CO on Ni/CeO_2 occurred at comparable rates [16]. Although Ni/CeO_2 anodes were susceptible to coking with methane [17,18], the addition of zirconia, however, may improve the coke tolerance of these anodes.

In this study the performance and stability of Ni/Ni–$Zr_{0.35}Ce_{0.65}O_{2-\delta}$ (ZDC) anodes were investigated and compared to Ni/YSZ anodes. Both anodes were tested in H_2 and in pure MeOH at 1073 K. Our objectives were to verify whether the presence of ZDC suppresses carbon deposition at zero fuel utilization and to verify whether coking is suppressed or reduced when the cell is operated at fuel utilizations higher than the thermodynamic carbon formation boundary [8]. To maintain a consistent microstructure, both anodes (Ni/YSZ and Ni/ZDC) were prepared by impregnating a porous YSZ structure with metal precursors. Steady-state polarization, electrochemical impedance spectroscopy (EIS), and potentiostatic measurements were used to characterize the performance and stability of these cells. Scanning electron microscopy was used to investigate the morphology of the anodes, while temperature-programmed oxidation was used to characterize carbon deposited on the anodes.

2. Materials and methods

2.1. Preparation of electrolyte, anode support, and cathode

A dense YSZ electrolyte layer was prepared by tape casting using commercial YSZ powders (TZ-8Y; Tosoh, Tokyo, Japan) according to the formulation of Table 1. The ingredients of the tape casting formula were dehydrated ethyl alcohol (Commercial Alcohols, Inc., Chattam, ON, Canada), toluene (ACS grade; VWR, Chester County, PA, USA), fish oil (Tape Casting Warehouse, Morrisville, PA, USA), and a polymer solution containing 19.5 wt% polyvinyl butyral (B79; Tape Casting Warehouse), 36.5 wt% butylbenzylphthalate (S160; Tape Casting Warehouse), 17.2 wt% dehydrated ethyl alcohol, and 26.9 wt% toluene.

Table 1
Tape cast formulations.

Component	Mass for dense YSZ (g)	Mass for porous YSZ (g)
Ethyl alcohol	7.67	8.50
Toluene	11.25	11.25
Fish oil	1.10	1.10
Polymer solution	20.50	20.50
YSZ	50.00	28.02
Corn starch	–	15.04
Graphite	–	6.95

A porous YSZ layer for the impregnation of the anode was obtained by adding corn starch (average particle size ~10 μm; generic brand) and graphite powder (−325 mesh; Alfa Aesar, Ward Hill, MA, USA) to the tape casting mix (Table 1). Green tapes of both the dense and porous electrolytes were laminated together and punched into disks 2.6 cm in diameter (see also [19]). Cells so obtained were sintered at 1773 K for 4 h using a heating rate of 2 K min^{-1} [20]. After sintering, the thicknesses of the dense and porous layers were approximately 50 and 70 μm, respectively (Fig. 1a). The apparent porosity of the porous layer was estimated as 60% based on Archimedes' method. The cathode was obtained by screen-printing a paste composed of α-terpineol (Alfa Aesar), LSM ($La_{0.8}Sr_{0.2}MnO_{3-\delta}$, Praxair Specialty Ceramics, Danbury, CT, USA), YSZ, and graphite powder (−325 mesh; Alfa Aesar) onto the dense surface of the YSZ electrolyte. The composition of the cathode was 47.7 wt% LSM, 43.2 wt% YSZ, and 9.1 wt% graphite. After firing at 1473 K for 2 h, the average thickness of the LSM cathodes was approximately 30 μm and the area was 0.21 cm^2.

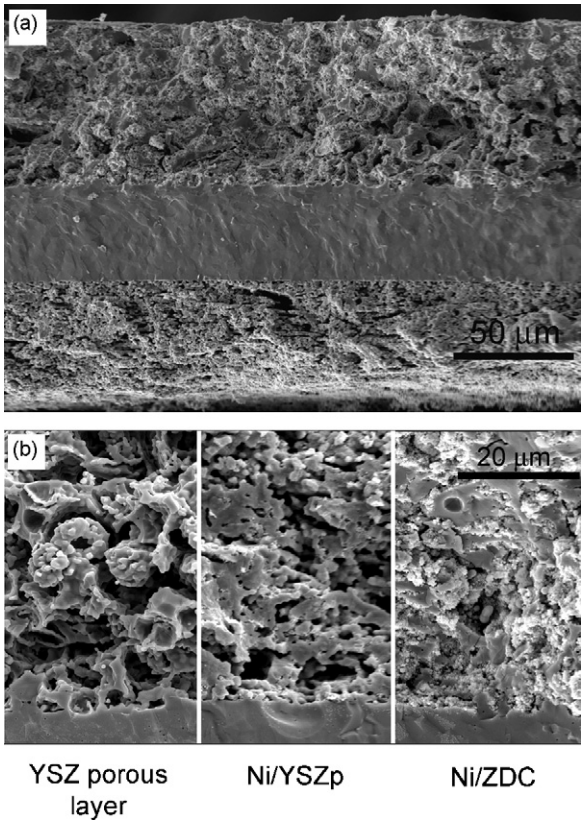

Fig. 1. SEM micrographs: (a) Ni/ZDC cross-section (anode at top of image); (b) porous YSZ layer and reduced Ni/YSZp and Ni/ZDC anodes before exposure to MeOH.

2.2. Preparation of impregnated anodes

Ni/YSZ anodes and Ni/$Zr_{0.35}Ce_{0.65}O_2$ (Ni/ZDC) anodes were obtained by impregnation of the YSZ porous layer with solutions consisting of metal nitrates in isopropyl alcohol using a modification of a procedure proposed elsewhere [21]. For the impregnated Ni/YSZ cells (hereafter referred to as Ni/YSZp), nickel was added to the porous YSZ layer with a 2 M solution of $Ni(NO_3)_2{\cdot}6H_2O$ (Alfa Aesar). Impregnated cells were dried at 343 K under vacuum for 15 min and then fired at 723 K for 60 min using heating and cooling rates of 2 and 5 K min^{-1}, respectively. This procedure was repeated until the weight of Ni was equivalent to approximately 40 wt% of the porous layer. NiO was reduced *in situ* using humidified H_2.

Ni/ZDC anodes were prepared in a similar manner. ZDC was deposited on the porous YSZ layer using an aqueous solution containing $ZrO(NO_3)_2{\cdot}xH_2O$ and $(NH_4)_2Ce(NO_3)_6$ (Alfa Aesar) at the calculated molar ratio. Cerium–ammonium nitrate precursor was selected to obtain a single ZDC phase at lower firing temperatures [22]. The presence of a single ZDC phase was verified by X-ray powder diffraction (XRD). ZDC powders were prepared by firing samples of the solution containing cerium and zirconium precursors at 723 K, and XRD patterns were obtained with a Rigaku powder diffractometer scanning between 10° and 80° using Cu Kα radiation. The XRD pattern shown in Fig. 2 presents the same peaks observed for ZDC solid solutions by Hartridge and Bhattacharya [23], confirming the presence of a single phase.

Impregnated cells were dried and then fired as described earlier for Ni/YSZp. The final ZDC content was approximately 30 wt%. Ni was added as described above until a loading of 40 wt% was reached. Both mass percents are with respect to the porous layer.

The cells have been named C1 through C8. The typical morphologies of the Ni/YSZp and Ni/ZDC cells after reduction are shown in Fig. 1b. An SEM image of the YSZ porous layer is also shown for comparison.

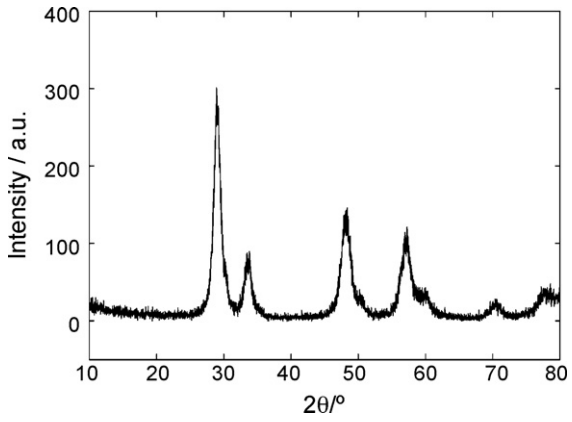

Fig. 2. XRD pattern of ZDC powders obtained after firing an aqueous solution of metal precursors at 723 K.

2.3. Experimental cell and set-up

The current collectors on the cathode side were platinum (Pt) wire (Omega Eng. Inc., Bergar, QC, Canada) attached using Pt paste (Engelhard, Iselin, NJ, USA). On the anode side, silver (Ag) wire (Alfa Aesar) and Ag ink (Alfa Aesar) were used. Part of the anode surface was masked using glass-sealing paste (4460, ESL Electro-Science, King of Prussia, PA, USA) to match the geometric area of the cathode (0.21 cm^2). The cell was attached to an alumina tube (diameter 13 mm, Vesuvius Ceramics, Carnegie, PA, USA) using glass-sealing paste cured on the cathode side with ceramic cement

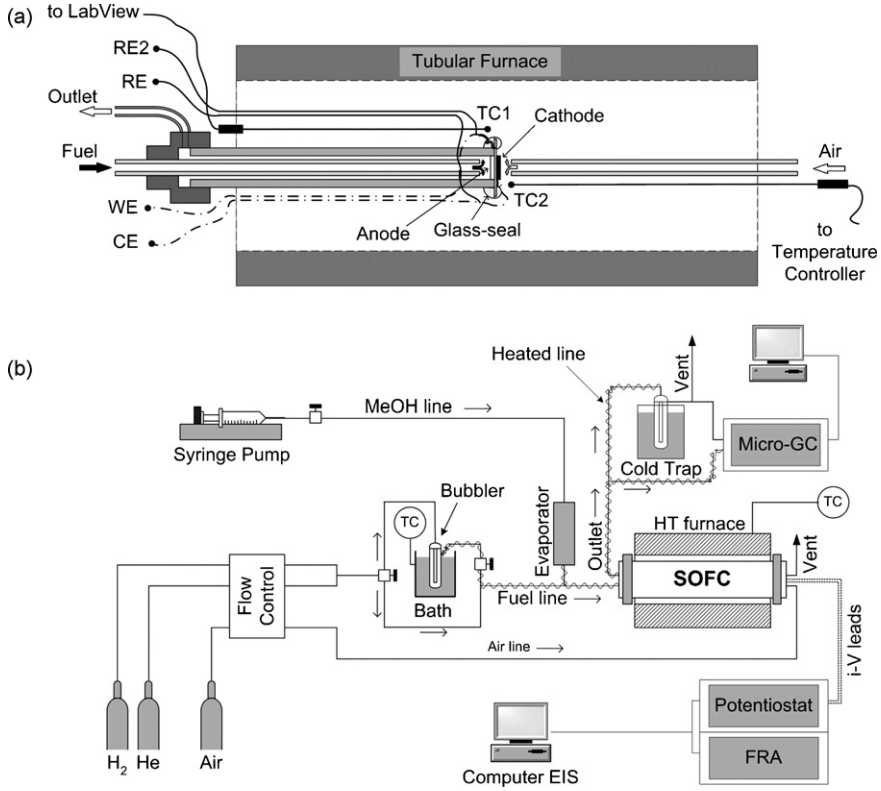

Fig. 3. Schematic of the (a) cell holder and (b) experimental set-up. WE and CE are the working and counter electrodes, RE and RE2 are the voltage references, and TC, TC1 and TC2 are thermocouples.

(Ultra-Temp 516, Aremco, Valley Cottage, NY, USA). Ag wires (Alfa Aesar) inserted in Nextel sleeves (Omega) were used as lead-wires; the wires were twisted to reduce stray-inductance during impedance measurements. Quartz tubes were used as fuel and air inlets in the cell arrangement of Fig. 3a. The H_2 flow rate was 50 mL min^{-1}, while the air-flow rate was 150 mL min^{-1}.

Pure liquid MeOH (water < 0.1 wt%) was injected directly to the anode compartment at 2 mL h^{-1} (1.373E−5 mol s^{-1}) through a capillary inlet tube (0.43/0.32 Lexis, Polymicro Technologies, AZ, USA) using a syringe pump (PHD 2000 Harvard Apparatus, Holliston, MA, USA). The outlet gases were directed to a gas chromatograph (mGC 3000 Agilent Technologies, Santa Clara, CA, USA) and to a cold trap kept at 200 K. The mGC has three channels (Molecular Sieve, Plot U, OV1) and was calibrated for the quantification of hydrogen (H_2), methane (CH_4), carbon monoxide (CO), carbon dioxide (CO_2), ethene (C_2H_4), ethane (C_2H_6), formaldehyde (HCHO), water (H_2O), and methanol (CH_3OH). The standard error for the chromatographic measurements was less than 2% for all species, except for HCHO and MeOH that was less than 5% for vapors. The quality of MeOH and the composition of the condensate from the cold trap were analyzed using a GC–MS (5975B-6890N Agilent Technologies). A schematic of the experimental set-up is shown in Fig. 3b.

2.4. Electrochemical testing

Steady-state polarization curves (i–V) and electrochemical impedance spectra (EIS) were measured using an electrochemical interface (1287 Potentiostat and 1260 Frequency response analyzer, Solartron Analytical, Farnborough, Hampshire, U.K.). Polarization curves were obtained from potentiostatic steps of 3 min taken every 50 mV. Impedance spectra were measured at equilibrium (OCV) and at different loads with AC amplitude of 20 mV in the frequency range of 0.01 Hz to 1 MHz. EIS results were validated by applying the Kramers–Kronig transformation (KKT) [24] in the linear implementation [25]. Lack of stability during the EIS measurement can be detected by comparing the residuals of the KKT to the error structure of the measurement [26,27]. In this study, the nominal errors of the electrochemical interface were used to detect instability in the KKT analysis. Long-term stability of the cells was determined at constant potential for periods of 12 h.

The typical testing procedure was as follows. First, cells were heated to 1073 K and tested in dry H_2 to verify that the sealing was adequate. Cells producing a stable voltage higher than 1.15 V in dry H_2 were exposed to humidified H_2 (approximately 4 vol%, bubbler temperature 301 K) and conditioned for at least 12 h before further measurements. After conditioning, cells were tested in pure MeOH at 1073 K.

2.5. Testing protocols

Eight cells were tested: four cells with Ni/YSZp anodes and four cells with Ni/ZDC anodes. Two cells of each type were tested to investigate the effectiveness of ZDC in suppressing coking at OCV. The remaining four cells were tested to verify whether operating the cells under load reduced coking compared to operation at OCV. In testing protocol-1, the cells were tested according to the following sequence: (1) cells were conditioned in H_2; (2) the fuel was switched to pure MeOH and the initial performance was determined; (3) cells were kept at open circuit in MeOH for 12 h while monitoring the voltage and outlet gas composition by GC; (4) the performance in MeOH was determined again; (5) the anode feed was switched to dry He while the cell was cooled to room temperature (Table 2). Protocol-2 was identical to protocol-1, except the cells were held at a constant voltage of 0.6 V for 12 h in the stability phase of the protocol (step 3).

Table 2
Testing protocols used in this study.

Stage	Fuel	Time (h)	Measurement type
Conditioning	H_2, 4% H_2O	24	Potentiostatic at 0.6 V
Initial performance	MeOH	–	Polarization, EIS
Stability	MeOH	12	Open circuit[a] or Potentiostatic at 0.6 V[b], GC
Final Performance	MeOH	–	Polarization, EIS
Cooling	He, dry	6	–

[a] Open circuit was used for protocol 1.
[b] Potentiostatic at 0.6 V was used for protocol 2.

2.6. Post-testing analysis

Tested anodes were broken into two parts: one part was used to examine the anode morphology using scanning electron microscopy (SEM, Philips ESEM-XL30) while the other part was characterized for carbon using temperature-programmed oxidation (TPO). The samples were gold-sputtered before SEM imaging. TPO experiments were carried out using 10 vol% O_2 in He with a flow rate of 50 mL min^{-1} STP. The temperature was ramped from room temperature to 1173 K at 10 K min^{-1} and the effluent gases were analyzed using a mass spectrometer (Cirrus 200 Quadrupole, MKS, Andover, MA, USA). The species monitored during the TPO were CO_2, O_2, CO, H_2O, and He. After each experiment the signal for CO_2 was calibrated using a 1 vol% CO_2 calibration mixture (Praxair), while the signal for H_2O was calibrated using 3 vol% H_2O in He.

3. Results

3.1. Performance and stability at zero fuel utilization

3.1.1. Ni/YSZp cells

An example of the polarization curves obtained in humidified H_2 and in pure MeOH at 1073 K with Ni/YSZp anodes (cells C1–C4) is shown in Fig. 4a. In both fuels, the polarization curves have a nonlinear region characterized mainly by activation losses (i < 0.1 A cm^{-2}), followed by a linear region where ohmic losses dominate (i > 0.1 A cm^{-2}). The activation losses are larger for MeOH than for H_2, while the slope of the ohmic region is steeper in H_2 indicating a larger ohmic resistance. These Ni/YSZp cells produced modest maximum power densities when compared to optimized anode-supported Ni/YSZ cells [6]. The results summarized in Table 3 show significant performance variability for Ni/YSZp cells, which is likely a result of the preparation procedure used.

Fig. 5 shows examples of the characteristic equilibrium impedance spectra obtained for a Ni/YSZp anode (cell C1). The complex plots obtained in humidified H_2, in MeOH initially, and in MeOH after 12 h of testing are shown in Fig. 5a, while the respective Bode plots are shown in Fig. 5b. The ohmic resistances (R_Ω, high frequency intercept in the complex plots) were 0.60 and 0.56 Ω cm^2 in H_2 and MeOH, respectively. The polarization resistance (anode + cathode) was ∼9 Ω cm^2 in H_2 while in MeOH the polarization resistance was ∼20 Ω cm^2. After 12 h of exposure to the pure alcohol, the impedance spectrum increased with decreasing frequency approaching a slope of ∼45° in the complex plane, similar to an infinite-length Warburg impedance [24]. The peak-frequency was approximately 500 Hz for H_2, and approximately 5 Hz in MeOH initially, which is a difference of 2 orders of magnitude between the characteristic relaxation times associated with the oxidation of these reactants. The spectra obtained for the other Ni/YSZp cell was similar, with comparable ohmic resistances but higher polarization resistances in both fuels. The EIS results obtained for these cells were validated by the linear KKT analysis. In general, the KKT was not satisfied for data obtained in

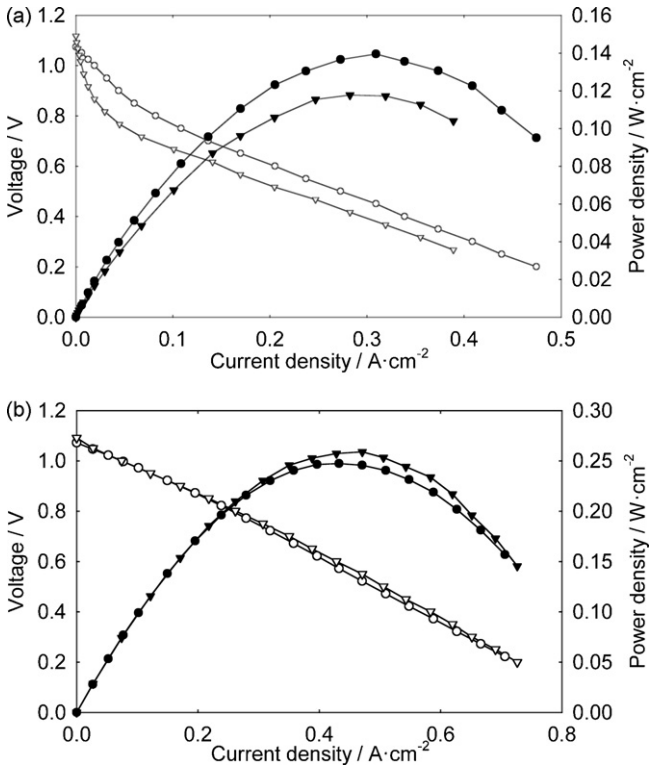

Fig. 4. Initial polarization (open symbols) and power density (closed symbols) curves at 1073 K in humidified H_2 (○, ●) and in MeOH (□, ▼) for (a) Ni/YSZp cell C1 and (b) Ni/ZDC cell C5.

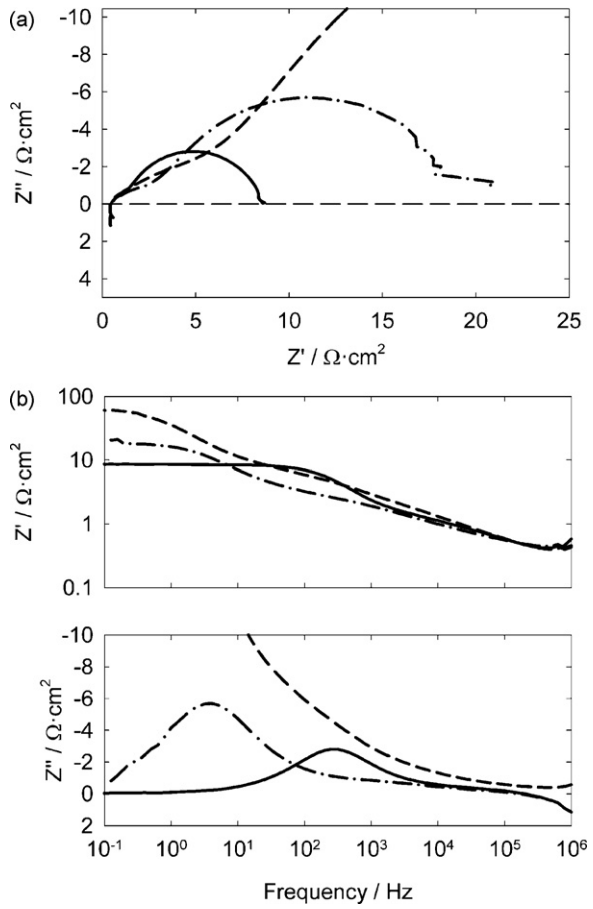

Fig. 5. Equilibrium impedance (a) complex plot and (b) Bode plots obtained in humidified H_2 (solid line), in MeOH initially (dash-dot), and in MeOH after 12 h (dashed) for Ni/YSZp cell C1.

MeOH. Specifically, the residual was higher than 1% for frequencies lower than ~1 Hz, indicating that the condition of stability was not satisfied during the EIS measurement (~5 min).

Fig. 6a shows the outlet gas composition, the measured OCV and the calculated cell voltage based on the measured gas composition as a function of time during the stability testing for the Ni/YSZp anode (cell C1). The main species detected were MeOH, H_2, and CO. Small amounts (≤1%) of HCHO, H_2O, and CH_4 were also detected, while trace amounts of C_2H_4 and C_2H_2 were only detected occasionally. CO_2 was not detected. Generally the partial pressure of MeOH decreased with time while the partial pressures of H_2 and CO increased. Although there was some scatter in the profiles, the

Table 3
Summary of performance and stability (at either OCV or 0.6 V) results obtained in pure MeOH at 1073 K for cells C1–C8.

	Ni/YSZp	OCV	Ni/YSZp	0.6 V	Ni/ZDC	OCV	Ni/ZDC	0.6 V
	C1	C2	C3	C4	C5	C6	C7	C8
Humidified H_2								
OCV (V)	1.074	1.070	1.067	1.076	1.072	1.064	1.069	1.072
Power (W cm^{-2})	0.139	0.075	0.127	0.094	0.247	0.209	0.233	0.229
R_Ω (Ω cm^2)	0.61	0.76	0.91	0.87	0.38	0.41	0.46	0.45
ASR[a] (Ω cm^2)	2.29	4.18	2.49	3.42	1.19	1.37	1.22	1.25
Methanol								
Initial OCV (V)	1.118	1.102	1.109	1.112	1.092	1.106	1.089	1.117
Initial power (W cm^{-2})	0.117	0.093	0.119	0.082	0.259	0.212	0.226	0.252
Initial R_Ω (Ω cm^2)	0.56	0.55	0.88	0.70	0.30	0.33	0.34	0.40
Initial ASR (Ω cm^2)	7.54	4.54	6.92	10.1	1.25	1.41	1.32	1.17
U_f during stability (%)	–	–	0.4	0.3	–	–	2.2	2.5
Final OCV (V)	1.078	1.076	1.069	1.077	1.099	1.085	1.087	1.102
Final power (W cm^{-2})	0.055	0.026	0.065	0.049	0.185	0.193	0.213	0.250
Final R_Ω (Ω cm^2)	0.59	1.32	0.94	1.01	0.31	0.33	0.32	0.42
Final ASR (Ω cm^2)	15.5	21.9	13.1	17.4	1.62	1.54	1.45	1.18
APD[b] (mW cm^2 h^{-1})	5	6	5	3	6	2	1	1
EDX carbon (wt%)[c]	41	45	36	42	5	3	2	2

[a] Average area specific resistance (ASR) according to the definition given in Ref. [39].
[b] Average performance decay (APD) calculated as the variation of power per unit time.
[c] Carbon on the pore surface determined by EDX (average atomic weight fraction calculated from the *K*-ratio, semi-quantitative).

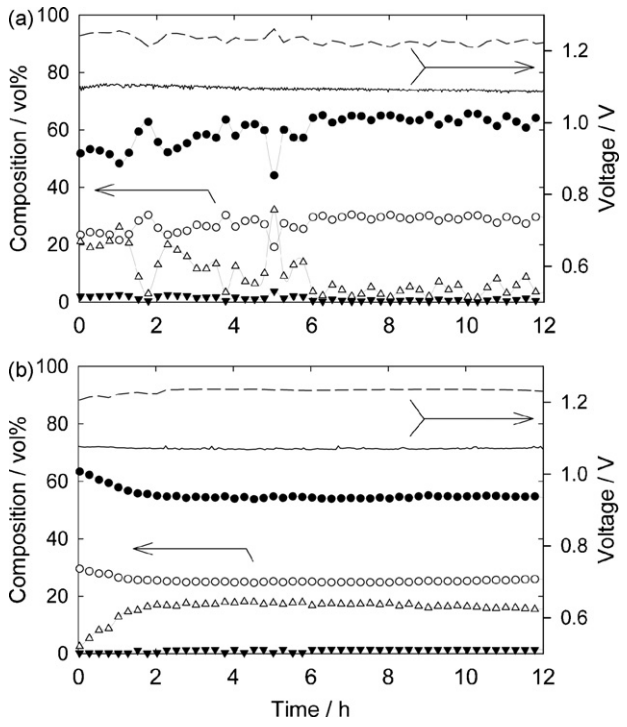

Fig. 6. Outlet composition (left ordinate) and voltage (right ordinate) versus time for cells Ni/YSZp cell C1 (a) and Ni/ZDC cell C5 (b). Species with concentration ≥1 vol% are: H_2 (●), CO (○), MeOH (□), and HCHO (▼). The solid lines represent the measured OCV, while the dashed lines are the calculated potentials corresponding to the measured composition.

relationship between the concentration of reactant (MeOH) and the concentration of the products H_2 and CO was consistent. A similar behavior has been observed for tape-cast Ni/YSZ catalysts exposed to MeOH [28]. The measured OCV was essentially constant at 1.080 V during the entire stability test in MeOH, although the OCV in MeOH during initial performance testing (immediately after testing in H_2, see Table 3) was approximately 1.120 V. The OCV calculated based on the outlet composition is almost 150 mV higher than the measured value, indicating that the gas phase composition at the electrochemically active surface (i.e., triple phase boundary) was different than the outlet gas phase composition. The composition profiles measured for the other Ni/YSZp anode (cell C2, not shown) were similar to that for cell C1, except that the MeOH concentration decreased more slowly.

After stability testing, the Ni/YSZp cells were tested again for performance and a significant decrease (~50%) in the maximum power density was observed (Table 3). At the end of the experiment the anodes were inspected visually and with SEM. The Ni/YSZp anode (cell C1) after testing is shown in Fig. 7a. Dust-like carbon deposits were present on the internal surface of the alumina cell holder up to 5–6 cm from the electrode. Part of these deposits were likely pyrolytic in nature, as shown in [28]. The surface of the anode was also covered with carbon; the cell easily crumbled when detached from the cell holder and essentially all of the mechanical integrity was lost.

Fig. 8 shows SEM micrographs of the Ni/YSZp anode (cell C1) after testing in MeOH at OCV. Comparing Fig. 8a and Fig. 1b (center image), the pores of the anode exposed to MeOH have been filled with amorphous carbon deposits. This result is corroborated by the EDX analysis, which shows a large carbon peak (inset in Fig. 8a). The micrograph shown in Fig. 8b shows an example of the extensive delamination of the electrode observed for the Ni/YSZp anode exposed to MeOH. EDX analysis indicates an average carbon concentration of ~40 wt% but the concentrations varied

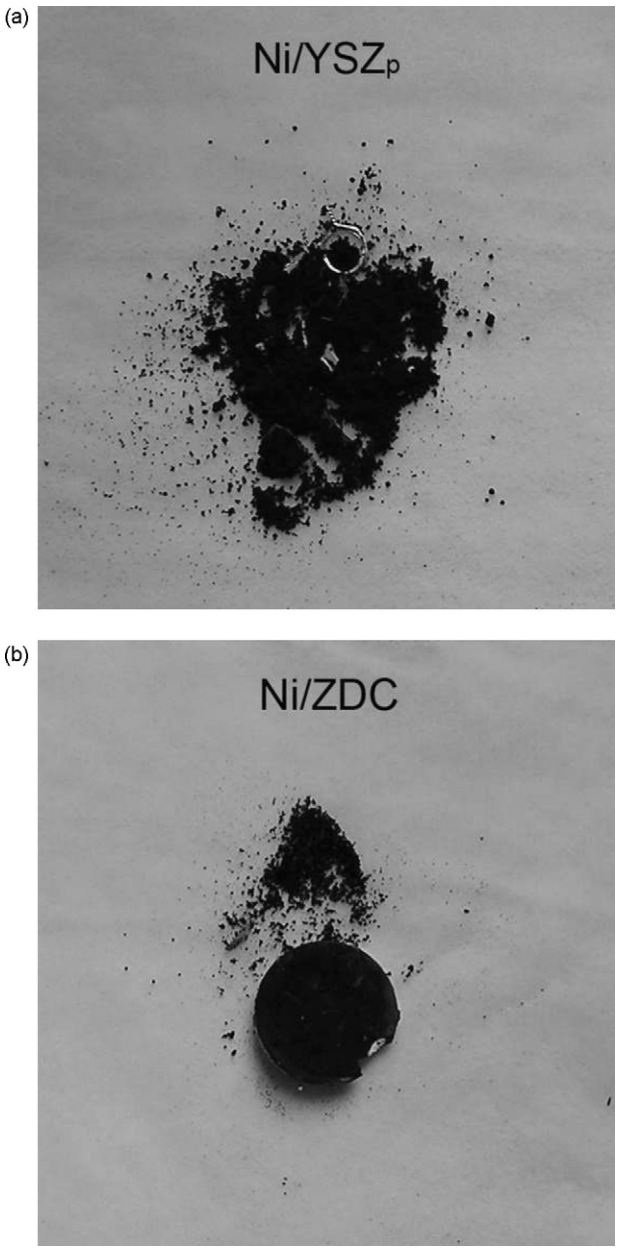

Fig. 7. Images of (a) Ni/YSZp cell C1 and (b) Ni/ZDC cell C5 after testing in MeOH for 12 h at 1073 K and OCV.

considerably between locations. EDX quantification provides only semi-quantitative results because the atomic weights of the components (e.g., C and metals) of the spent anode samples are very different. The TPO profile obtained for the Ni/YSZp anode (cell C1) is shown in Fig. 9a. The profile has a peak at 915 K, and a shoulder at 1031 K. There was not a peak for H_2O, indicating that the hydrogen content of the carbon deposits was negligible.

3.1.2. Ni/ZDC cells

Fig. 4b shows an example of the polarization curves obtained with Ni/ZDC anodes (cells C5–C8). In general the performance of Ni/ZDC was higher than Ni/YSZp, although the Ni content was nominally the same (note the different scales on the power density curves in Fig. 4a and b). After less than one hour of exposure to pure MeOH, the performance of a Ni/ZDC anode (cell C5) was slightly higher than in H_2, consistent with results obtained previously with Ni/CeO_2 anodes [16]. In both fuels, the polarization

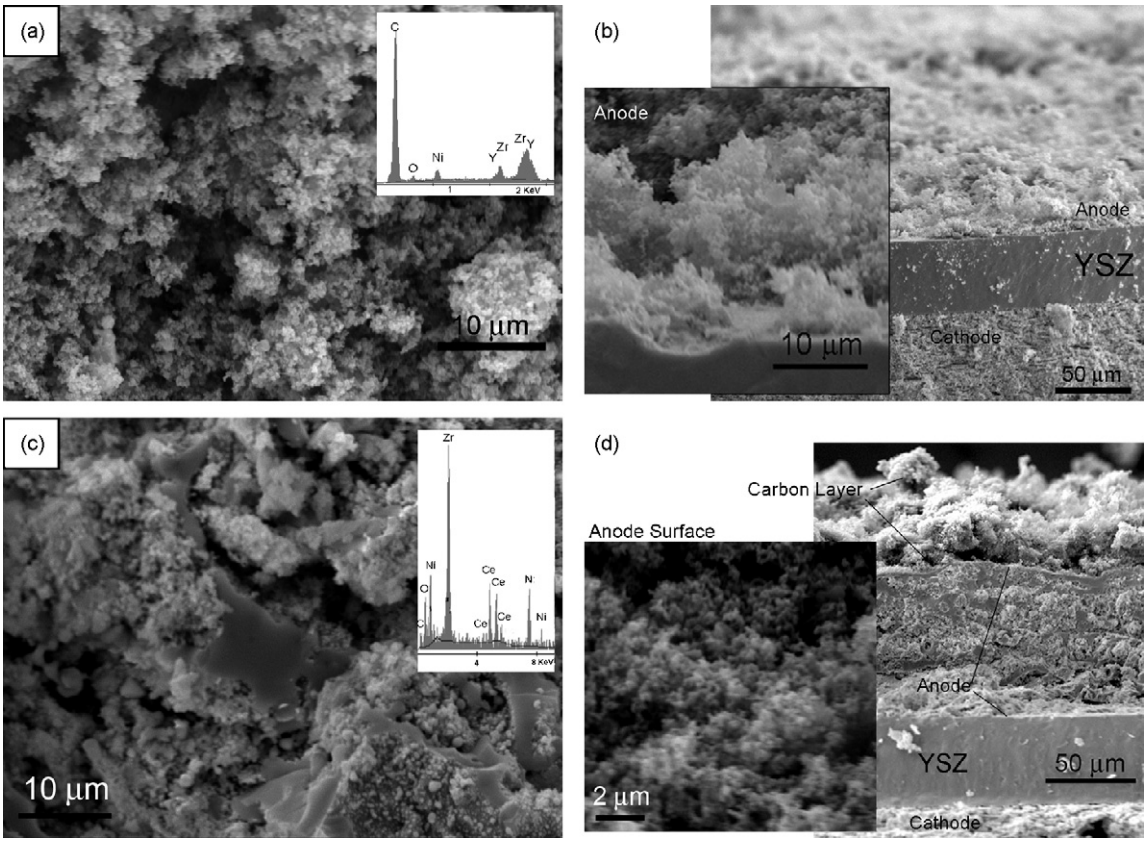

Fig. 8. SEM micrographs of (a) pore surface of Ni/YSZp anode after 12 h of testing in MeOH at OCV, EDX profile is shown in the inset; (b) cross-section of the Ni/YSZp cell showing delamination of electrode; (c) pore of a Ni/ZDC anode after 12 h exposure to MeOH at OCV, EDX profile is shown in the inset; (d) cross-section of the Ni/ZDC cell showing a carbon layer on the external surface of the electrode, the inset is an enlargement of carbon deposited on the surface.

curves were essentially linear over the entire current range tested, indicating that ohmic losses were likely dominating. The performance variability for Ni/ZDC anodes was smaller than for Ni/YSZp anodes (Table 3).

Fig. 10 shows the equilibrium impedance spectra measured for a Ni/ZDC anode (cell C5) in H_2 (solid lines) and MeOH (dash-dot lines). The complex spectrum measured in H_2 (Fig. 10a) contains one depressed arc with a peak frequency at approximately 200 Hz (Fig. 10b), whereas the spectrum obtained in MeOH contains two arcs (Fig. 10a) with peak frequencies at 100 and ~0.02 Hz for the first and second arc, respectively. As for Ni/YSZp anodes, the ohmic resistance was lower in MeOH than in H_2 (0.30 and 0.38 $\Omega\,cm^2$, respectively). For this cell, the polarization resistance in H_2 was 0.94 $\Omega\,cm^2$, while in MeOH the spectrum was not closed at the low frequencies. The impedance spectrum after 12 h in pure MeOH for this cell (C5, not shown) was almost identical to the initial spectrum, except that the low frequency arc was noisier. All Ni/ZDC cells had similar impedance spectra, and the EIS data satisfied the KKT, with residual errors of less than 1% within the entire bandwidth.

Fig. 6b shows the time profile of the outlet gas composition, measured OCV and calculated cell voltage for the Ni/ZDC anode (cell C5) during the stability testing at open circuit conditions. The concentration of MeOH increased from 0 to approximately 17 vol% within the first 2 h, while the concentration of H_2 and CO decreased to ~54 and 25%, respectively, over the same time period. After 2 h at OCV, the outlet-gas composition and calculated OCV were stable. The measured OCV was constant at ~1.09 V. The measured outlet composition was 19% MeOH, 55% H_2 and 24% CO. The calculated potential (Nernst equation) for such composition is ~1.22 V. Thus, as for Ni/YSZp anodes, the potential calculated based on the outlet composition was approximately 120 mV higher than the measured OCV. The composition profiles measured for the other Ni/ZDC anodes (cell C6) were similar. After stability testing the performance decrease of the Ni/ZDC cells were 28 and 9%, which was significantly smaller than for Ni/YSZp cells (Table 3).

Fig. 7b shows a Ni/ZDC anode (cell C5) after testing. Loose carbon deposits were present on the anode surface and also on the surface of the sample holder. The structure of the cells, however, was not as fragile as for Ni/YSZp and the cell could be removed from the sample holder without crumbling. Fig. 8c and d shows micrographs of a pore and the cross-section of the Ni/ZDC anode (cell C5) after 12 h at OCV in MeOH. The pores in the cross-section appear to be free of carbon deposits (Fig. 8c compared to Fig. 1b), but ~18% C was detected in some locations by EDX. The intensity of the EDX C-peak was always smaller for Ni/ZDC anodes than for Ni/YSZp anodes (see insets in Fig. 8a and c). A ~50 µm thick carbon layer covered the anode surface (Fig. 8d), while no damage was visible on the anode microstructure.

Fig. 9b shows the TPO profile for the Ni/ZDC anode (cell C5) after 12 h in MeOH at OCV or under load. After operation at OCV, less carbon was deposited than on the Ni/YSZp anode and this carbon was slightly more reactive. That is, the peak temperature is 882 K (compared to >900 K for Ni/YSZp). When current is flowing, no carbon was deposited on the Ni/ZDC anode as will be discussed below.

3.2. Performance and stability under load

3.2.1. Ni/YSZp cells

The polarization curves of Ni/YSZ_p cells tested for stability under load (cells C3 and C4) were essentially the same as those obtained for cells tested at OCV. Results are summarized in Table 3. The initial equilibrium impedance spectra of cells C3 and C4 were also

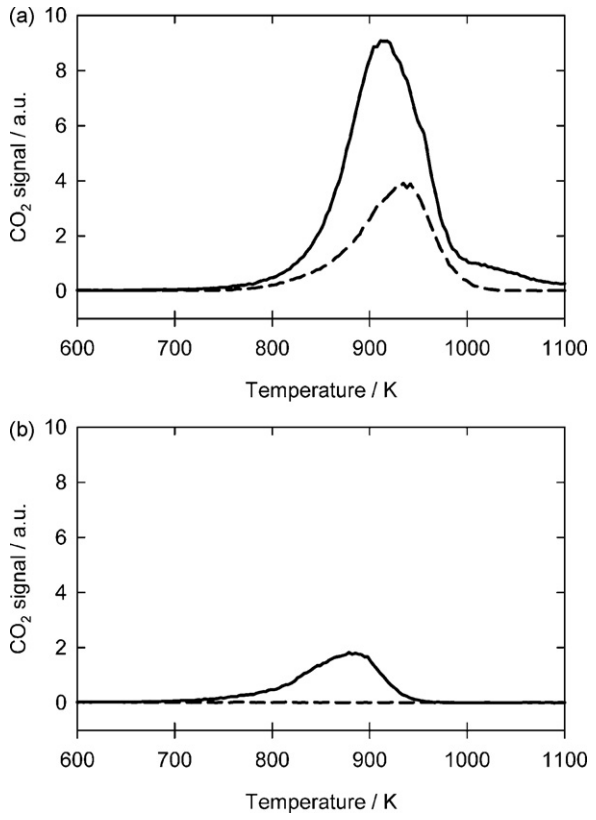

Fig. 9. TPO profiles of (a) Ni/YSZp cell C1 and (b) Ni/ZDC cell C5 after 12 h in MeOH and OCV (solid line) and after 12 h in MeOH at 0.6 V (dashed line).

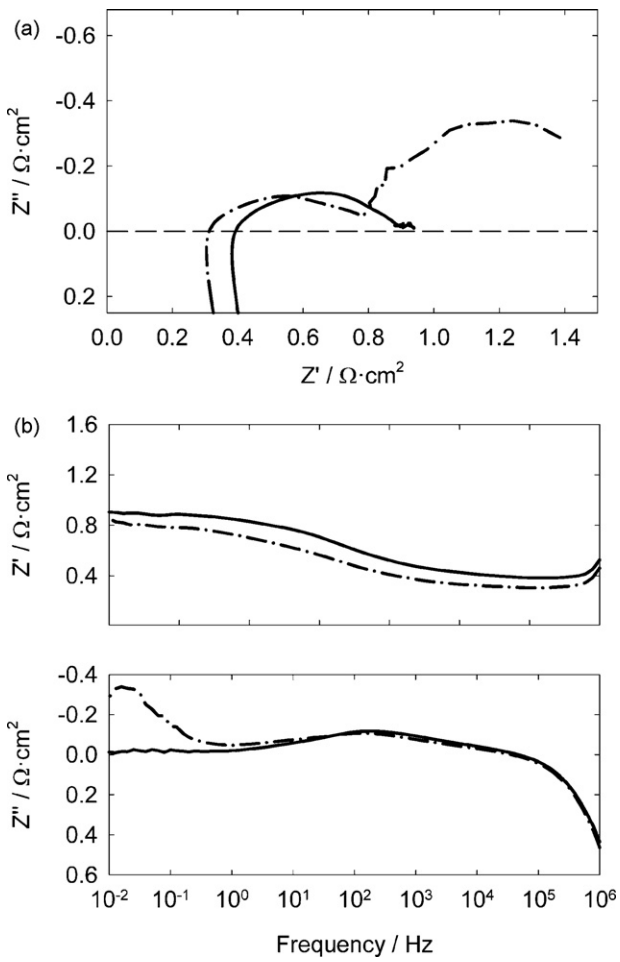

Fig. 10. Equilibrium impedance (a) complex plot and (b) Bode plots obtained in humidified H_2 (solid line), and in MeOH initially (dash-dot) for Ni/ZDC cell C5.

similar to the spectra shown in Fig. 5. To better understand the limiting processes of these cells, the impedance spectra were measured for different loads and the results are shown in Fig. 11a. The ohmic resistance did not change with load, while the polarization resistance decreased with increasing load, indicating some activation limitation of the anode, consistent with the polarization behavior of Fig. 4a. The peak frequency of the main arc increased with increasing loads, which is also expected in the case of activation limitations. Similar to Fig. 5a, the impedance spectra of Ni/YSZp cells measured in MeOH at 0.6 V (not shown) increased both in real and complex components with decreasing frequency. The impedance points for frequencies less than 0.1 Hz were noisy, and generally the residual obtained from the linear KKT was larger than 1%, indicating that the condition of stability was not satisfied.

Fig. 12a shows the outlet gas composition profile and the power density measured at 0.6 V as a function of time. The main species detected were MeOH, H_2, and CO, with small amounts (<2%) of HCHO, H_2O, and CO_2. The concentration profiles were noisy as for cells tested at OCV (Fig. 6a), and the apparent MeOH concentration decreased with time, while the concentrations of H_2 and CO increased. Both H_2O and CO_2 were detected but at concentrations lower than 2%. The power density measured at 0.6 V decayed with time, and for cell C3 was ~50 mW cm^{-2} after 12 h. The estimated fuel utilization (calculated from the MeOH flow rate and the measured current) was 0.4%, which was within the thermodynamic carbon formation region [8].

The SEM micrograph of a Ni/YSZp anode tested at constant load is shown in Fig. 13a. Amorphous carbon deposits covered the anode pores and surface, and several portions of the electrode were delaminated. In fact, there was no visible difference between anodes tested at OCV and under load. EDX results showed high concentrations (>30%) of C in the pores and on the surface of cell C4. Fig. 9a shows the TPO profile for a Ni/YSZp anode (C4) tested under load. The CO_2 signal has a peak 935 K, while H_2O was not detected. The height of the peak was lower than for cell C1; the same mass of sample was used in each TPO analysis.

3.2.2. Ni/ZDC cells

The polarization curves for Ni/ZDC cells tested under load (C7 and C8) were similar to the curves in Fig. 4b; likewise, the equilibrium impedance was similar to that in Fig. 5. Fig. 11b shows the impedance of Ni/ZDC cell C8 measured in H_2 at different loads. The ohmic resistance of the Ni/ZDC cells increased slightly with increasing load. Also the polarization resistance increased with load, while the peak frequency of the main arc did not change significantly. This behavior, opposite of that observed for Ni/YSZp, indicates that the electrochemical oxidation was not limiting the anode performance, but rather charge transport in the ZDC layer was likely the limiting factor. The impedance spectra measured at 0.6 V in MeOH (not shown) were similar to the spectra of Fig. 11b. As seen also in Fig. 10, a second semicircle was visible at lower frequencies.

Fig. 12b shows the gas composition and power density time profiles for a Ni/ZDC cell (cell C8) operated under load. The species detected at the outlet were the same as that observed for cells tested at OCV (Fig. 6b), but the average conversion of MeOH was lower (~10%, compared to ~15% at OCV). The concentration profiles were less stable than in Fig. 6b. The average power density for cell C8 was ~240 mW cm^{-2} and the calculated fuel utilization was ~2.2%, indicating that theoretically carbon deposition was not favored. The cell performance for Ni/ZDC cells in MeOH after stability testing was similar to or slightly higher than the initial performance (Table 3).

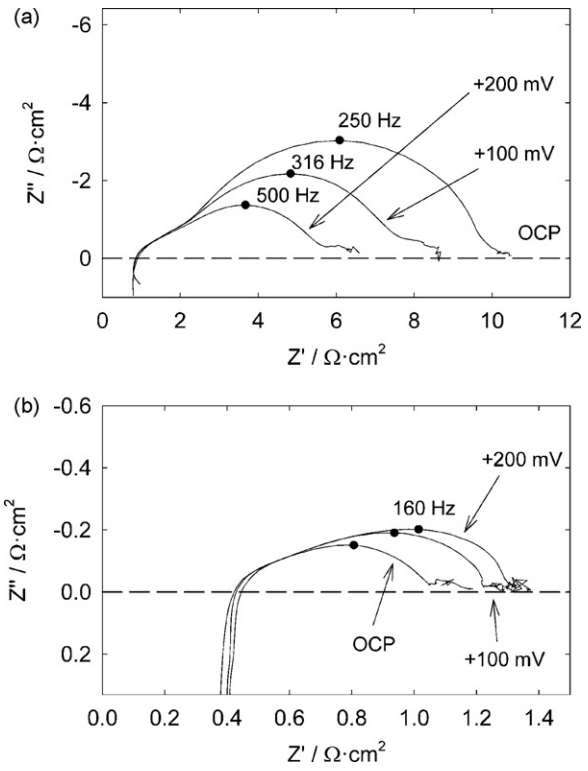

Fig. 11. Complex plot of the impedance spectra for different loads in humidified H_2 at 1073 K for (a) Ni/YSZp cell C3 and (b) Ni/ZDC cell C8. Peak-frequencies are indicated by the solid markers and labeled. Frequency range shown for all spectra is 0.01 Hz to 1 MHz.

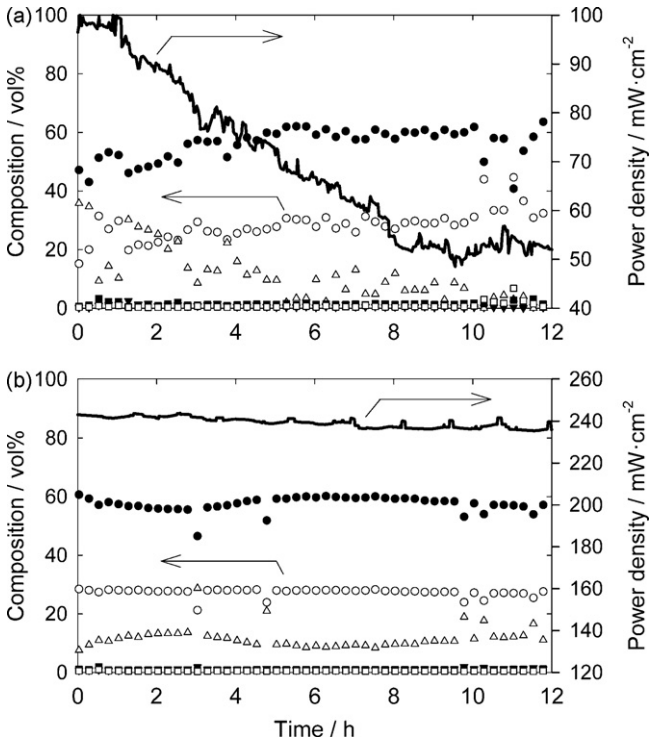

Fig. 12. Outlet composition (left ordinate and symbols) and power density (right ordinate and lines) versus time for (a) Ni/YSZp cell C3 and (b) Ni/ZDC cell C8 operated with a MeOH feed at 1073 K and 0.6 V. Species shown are: H_2 (●), CO (○), MeOH (△), HCHO (▼), CO2 (■), and H_2O (□).

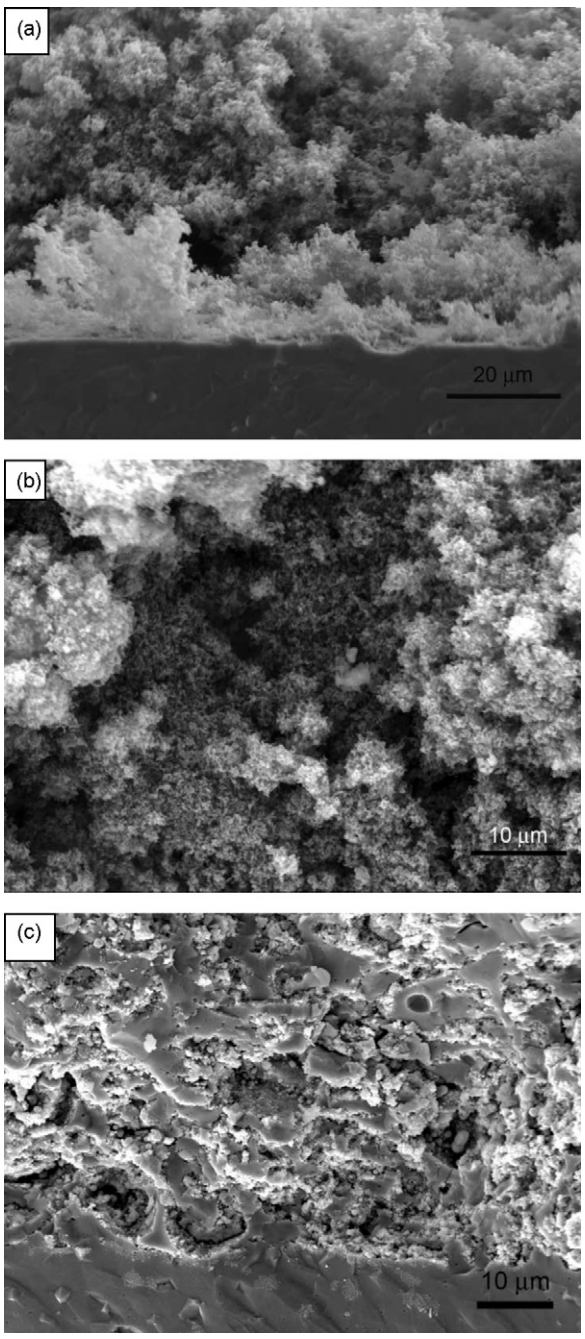

Fig. 13. SEM micrographs of (a) Ni/YSZp cell C5 (cross-section) after 12 h of testing in MeOH at 0.6 V; (b) Ni/ZDC cell C8 (cross-section) after 12 h of testing in MeOH at 1073 K and 0.6 V and (c) carbon deposits on the surface of cell in (b).

Although there was no performance degradation, carbon deposits were still observed (by visual inspection) on the surface of tested anodes. Fig. 13b and c show the SEM micrographs of the cross-section and surface, respectively, of a Ni/ZDC anode (cell C8) tested in MeOH under load. The cross-section of the anode appears relatively clean (Fig. 13b) although a small carbon signal was detected by EDX (not shown). Carbon deposits were visible in isolated spots on the anode surface. Fig. 13c shows the morphology of these surface deposits. As mentioned previously, there was no CO_2 evolved from the Ni/ZDC (cell C8) operated under load during the TPO analysis (Fig. 9b).

4. Discussion

One of the objectives of this study was to compare the influence of ZDC on Ni/YSZ anodes exposed to pure MeOH. Based on the results (Figs. 7, 9 and 13), ZDC was effective in reducing the carbon deposited on the anodes both at open circuit and under load (0.6 V). The higher performance of the Ni/ZDC anodes (Table 3 and Fig. 4) was likely due to the mixed conducting properties of ZDC. The ZDC phase provides a pathway for the conduction of electrons so that isolated Ni particles in the Ni/ZDC anode can still function electrocatalytically, while in Ni/YSZ anodes isolated Ni particles only provided sites for the catalytic decomposition, where coke is likely to accumulate. Further improvements in preventing carbon deposition could be achieved by optimizing the electrode microstructure, while stability to coking could be improved by doping the anodes with coke-inhibitors such as K and Ag as suggested by theoretical studies [29–31].

Although others [6,7] showed that Ni/YSZ anodes can operate with pure MeOH without coking, it is likely that the absence of coking was a consequence of the specific conditions used. Namely, at high fuel utilization and high temperatures carbon formation can be inhibited. In a practical setting in which an SOFC may be operated at a range of loads, including OCV, thus, the direct utilization of MeOH could lead to irreversible deactivation of the Ni/YSZ anodes after longer term operation.

After stability testing at OCV, carbon was deposited on both Ni/YSZp and Ni/ZDC, as expected from thermodynamic calculations. However, the performance of the Ni/ZDC cells was less impaired, and the carbon deposits were visible only on the external surfaces of these electrodes. Whereas the microstructure of Ni/ZDC anodes was not damaged by carbon, the Ni/YSZp anodes became delaminated from the electrolyte. Coked Ni/YSZp anodes were fragile likely because the deposited carbon resulted in metal dusting [32]. TPO profiles indicated that carbon deposits were more reactive (i.e., removed at a lower temperature) on Ni/ZDC than Ni/YSZp. Previous studies [33] have shown that the presence of ceria influences the type of carbon formed on Ni anodes exposed to methane. Carbon deposits were not quantified by TPO but EDX results showed that more carbon was present on Ni/YSZp anodes and also that the pores of Ni/ZDC anodes were relatively clean.

Consistent with other results [6,7], less carbon was deposited when the anodes were tested under load (Figs. 9 and 13). The performance of the Ni/ZDC was sufficiently high that the fuel utilization was slightly above the carbon deposition boundary (2.5% versus 2.1%). Although no carbon was detected with TPO, some carbon was detected with SEM/EDX analysis on the Ni/ZDC anodes. Carbon deposits were evident on the Ni/YSZp anodes with both TPO and SEM/EDX analyses.

The higher stability of Ni/ZDC cells was evident particularly considering that the initial performance in MeOH was maintained for both cells during 12 h in MeOH (Figs. 6 and 12). The gas phase concentration profiles at the outlet of the cell during testing at OCV (Fig. 6b) were stable after 2 h on stream for the cells with Ni/ZDC anodes, but were considerably less stable for cells with Ni/YSZp anodes. Similar trends were observed in a study on the decomposition of MeOH ex-situ on Ni/CeO_2 and Ni/YSZ catalysts [9], likely because of the similar catalytic properties of these materials for the decomposition of MeOH.

Not only was the performance of the Ni/YSZp anodes unstable but there was also poor reproducibility between the prepared anodes. The lack of electronic conductivity is most likely the cause of the performance variability between samples for Ni/YSZp cells. The performance of Ni/ZDC cells was more consistent, likely because the presence of ZDC results in less variability of the overall conductivity of the anode. In the Ni/YSZp anodes, the only conductive phase was Ni, and the Ni content was close to the conductivity threshold (according to percolation theory) such that the anode conductivity was more sensitive to the preparation method.

The OCV measured in MeOH could be a result of a mixed potential established through the anode, but more likely reflected the local composition at the functional layer. Thus, the difference between the measured and calculated voltages of ~120 mV (Figs. 6 and 12) was an indication that the gas composition at the outlet was different from the composition at the anode functional layer. The measured OCV was close to the value calculated assuming that equilibrium composition for MeOH decomposition was reached (~1.08 V for the equilibrium composition 62.9 mol% H_2, 29.5% CO, 2.5% H_2O, 1.9% CH_4, 1.3% CO_2, and 1.9% C at 1073 K, see [8]), supporting our previous hypothesis [9] that the gas phase in the proximity of the active layer is close to equilibrium. Aside from the concentration gradient within the anode, pyrolysis reactions within the sample holder could have also contributed to the difference between the calculated and measured OCV. The gas composition profiles at the outlet of the cell measured under load were essentially similar to those obtained at OCV, likely because of the low fuel utilizations. Peaks for H_2O and CO_2 were identified in the chromatograms, but the concentration of these species remained lower than 2%.

EIS results contained information both on the limiting processes and stability of Ni/YSZp and Ni/ZDC electrodes (Figs. 5, 10 and 11). The variation of the impedance spectra with load for Ni/YSZp cells in H_2 (Fig. 11a) indicated that the electrochemical oxidation was limiting the electrode performance. As discussed previously, this result was likely a consequence of the non-optimized microstructure and resulting poor electronic conductivity (i.e., smaller TPB) of these anodes. According to the KKT analysis impedance spectra collected during operation in MeOH for Ni/YSZp cells did not satisfy the stability condition. In addition, the ohmic resistance in the impedance spectra decreased when the fuel changed from H_2 to MeOH. Both of these results are consistent with carbon being deposited on the anodes [34].

Ni/ZDC cells exhibited a characteristic impedance behavior both in H_2 and MeOH. The increase of polarization resistance with load seen in Fig. 11b could be related to the electrochemical oxidation of H_2 and/or CO on the ZDC surface, as observed in three-electrode experiments [35]. A second arc with peak-frequency at ~0.02 Hz was observed in the equilibrium impedance spectra in MeOH. The possible causes of this feature are: gas-conversion within the volume of the sample holder contiguous to the electrode surface [36]; gas-diffusion within the electrode/current collector [37]; gas and Knudsen diffusion through electrode. The characteristic resistance and peak-frequency produced by gas-conversion in the case of H_2 fuel can be predicted as proposed in [36]. For the setup and conditions used in this study these are ~0.11 $\Omega\,cm^2$ and ~0.16 Hz, respectively. However, the predicted gas-conversion arc was not present in the impedance spectrum of H_2 (solid line in Fig. 10a).

Similarly, resistance and peak-frequency generated by gas-diffusion can be predicted as proposed in [37]. Assuming that the low frequency arc was caused by diffusion through the anode, it is possible to calculate the ratio of the effective diffusivity to the diffusion length required to produce the size and peak-frequency observed in MeOH (~0.8 $\Omega\,cm^2$ and ~0.02 Hz, dashed line in Fig. 10a), which should be $\sim 5 \times 10^{-3}\ m\,s^{-1}$. For a length equivalent to the electrode thickness results in a diffusivity of $\sim 10^{-7}\ m^2\,s^{-1}$. Such a small diffusivity would be possible only if Knudsen diffusion is predominant with an effective pore diameter of ~20 nm, which is not in agreement with the microstructure observed by SEM. Finally, the low frequency arc observed in MeOH for Ni/ZDC cells could be related to the coupled effect of MeOH decomposition, convection/diffusion, and electrochemical oxidation of some

decomposition products. Although a specific model to verify this hypothesis is not available yet, this could be the actual origin of the observed low-frequency arc, particularly considering that the results of Fig. 10b indicate that equilibrium of decomposition was likely reached in the proximity of the anode surface, in which case three molecules were produced for each MeOH molecule reacted generating a convective flow away from the anode surface. Thus, the small effective diffusivity calculated could be in fact the result of the volume increase produced by MeOH decomposition.

In general EIS results indicate that the processes limiting the performance of Ni/ZDC anode with pure MeOH are very different from those limiting Ni/YSZp anodes, and these processes could be the main cause of the improved stability observed.

5. Conclusions

The direct utilization of MeOH was tested on impregnated Ni/YSZ and Ni/ZDC anodes for SOFC. Stability was tested at OCV to verify and compare the resilience of these anodes at the most severe coking conditions, and also under load to verify that the presence of oxygen ions and/or water (produced by electrochemical oxidation) reduces coking. The results verified that Ni/ZDC anodes were more stable than Ni/YSZp anodes for the direct utilization of MeOH at 1073 K, both at OCV and under load. Under load, the performance of the Ni/ZDC anode was essentially stable over 12 h.

ZDC has a positive effect on the performance, similar to ceria [38], likely because of the increased conductivity within the anode. The presence of ZDC also influenced the type of carbon that formed such that the carbon was more reactive and could be removed without complete destruction of the anode microstructure. Operation under load reduced the amount of carbon formed on both anodes. The Ni/ZDC anode had relatively little carbon after operation with MeOH for 12 h at 0.6 V. The Ni/YSZp anode delaminated when operated at OCV for 12 h with MeOH. Under load, the performance of Ni/YSZp anode degraded substantially (100–50 mW cm^{-2} over 10 h).

EIS results indicate that performance on Ni/YSZp anodes was dominated by activation overpotential, while on Ni/ZDC the conduction of O^{2-} in ZDC is likely dominating. The higher stability in pure MeOH of Ni/ZDC is also reflected on the stability of EIS measurements. The characteristic low-frequency arc observed in the equilibrium impedance of Ni/ZDC cells tested in pure MeOH could be related to catalytic decomposition of MeOH on the anode.

Acknowledgements

This work was financed with a Natural Sciences and Engineering Research Council (NSERC) grant. The authors are grateful to Dr. Ryan Clemmer for helping with tape casting methods. M.C. is grateful to NSERC and Killam Trust for financial support.

References

[1] S.C. Singhal, K.E. Kendall, High Temperature Solid Oxide Fuel Cells—Fundamentals, Design and Applications, 1st ed., Oxford, UK, 2003.
[2] S.C. Singhal, Solid State Ionics 152 (2002) 405–410.
[3] G.A. Olah, Beyond oil and gas: the methanol economy, Wiley-VCH Weinheim, Germany, 2006.
[4] W.H. Cheng, H.H. Kung, Methanol production and use, Marcel Dekker, Inc., New York, 1994.
[5] K. Sasaki, Y. Teraoka, J. Electrochem. Soc. 150 (2003) A878–A884.
[6] Y. Jiang, A.V. Virkar, J. Electrochem. Soc. 148 (2001) A706–A709.
[7] K. Sasaki, H. Kojo, Y. Hori, R. Kikuchi, K. Eguchi, Electrochemistry (Denki Kagaku, Japan) 70 (2002) 18–22.
[8] M. Cimenti, J.M. Hill, J. Power Sources 186 (2009) 377–384.
[9] M. Cimenti, J.M. Hill, J. Power Sources 195 (2010) 54–61.
[10] N. Sammes, L. Varadaraj, Electrochemistry (Denki Kagaku, Japan) 63 (1995) 41–46.
[11] D.J.L. Brett, A. Atkinson, D. Cumming, E. Ramirez-Cabrera, R. Rudkin, N.P. Brandon, Chem. Eng. Sci. 60 (2005) 5649–5662.
[12] T. Kim, K. Ahn, J.M. Vohs, R.J. Gorte, J. Power Sources 164 (2007) 42–48.
[13] M. Sugiura, Catal. Surv. Asia 7 (2003) 77–87.
[14] Z. Zhang, Y. Zhang, Z. Mu, P. Yu, X. Ni, S. Wang, L. Zheng, Appl. Catal. B 76 (2007) 335.
[15] K.A. Pokrovski, A.T. Bell, J. Catal. 241 (2006) 276.
[16] M. Cimenti, J.M. Hill, Electrochem. Soc. Trans. 7 (2007) 1591.
[17] M.L. Toebes, J.H. Bitter, A.J. van Dillen, K.P. de Jong, Catal. Today 76 (2002) 33.
[18] H. Kim, C. Lu, W.L. Worrell, J.M. Vohs, R.J. Gorte, J. Electrochem. Soc. 149 (2002) A247–A250.
[19] M. Cimenti, J.M. Hill, Asia-Pac. J. Chem. Eng. 4 (2009) 45–54.
[20] S.F. Corbin, X. Qiao, J. Am. Ceram. Soc. 86 (2003) 401–406.
[21] R.J. Gorte, H. Kim, J.M. Vohs, J. Power Sources 106 (2002) 10–15.
[22] S. Letichevsky, C.A. Tellez, R.R.D. Avillez, M.I.P.D. Silva, M.A. Fraga, L.G. Appel, Appl. Catal. B 58 (2005) 203.
[23] A. Hartridge, A.K. Bhattacharya, J. Phys. Chem. Solids 63 (2002) 441–448.
[24] M.E. Orazem, B. Tribollet, Electrochemical Impedance Spectroscopy, Wiley-Interscience, Hoboken, New Jersey, 2008.
[25] B.A. Boukamp, J. Electrochem. Soc. 142 (1995) 1885–1894.
[26] P. Agarwal, M.E. Orazem, L.H. Garcia-Rubio, Electrochim. Acta 41 (1996) 1017.
[27] P. Agarwal, M.E. Orazem, L.H. GarciaRubio, J. Electrochem. Soc. 142 (1995) 4159–4168.
[28] M. Cimenti, J.M. Hill, J. Power Sources (2009) 2009, accepted 6 July.
[29] M. Itome, A.E. Nelson, Catal. Lett. 106 (2006) 21–27.
[30] H.S. Bengaard, J.K. Norskov, J. Sehested, B.S. Clausen, L.P. Nielsen, A.M. Molenbroek, J.R. Rostrup-Nielsen, J. Catal. 209 (2002) 365–384.
[31] N.V. Parizotto, K.O. Rocha, S. Damyanova, F.B. Passos, D. Zanchet, C.M.P. Marques, J.M.C. Bueno, Appl. Catal. A 330 (2007) 12.
[32] V. Alzate-Restrepo, J.M. Hill, Carbon deposition on Ni/YSZ anodes exposed to CO/H2 feeds, J. Power Sources 195 (2010) 1344–1351.
[33] H. He, J.M. Hill, Appl. Catal. A 317 (2007) 284.
[34] S. McIntosh, H.P. He, S.I. Lee, O. Costa-Nunes, V.V. Krishnan, J.M. Vohs, R.J. Gorte, J. Electrochem. Soc. 151 (2004) A604–A608.
[35] M. Cimenti, Direct utilization of methanol and ethanol in solid oxide fuel cells. Ph.D. Thesis. University of Calgary, Calgary (Canada). 2008.
[36] S. Primdahl, M. Mogensen, J. Electrochem. Soc. 145 (1998) 2431–2438.
[37] S. Primdahl, M. Mogensen, J. Electrochem. Soc. 146 (1999) 2827–2833.
[38] R.J. Gorte, J.M. Vohs, Novel, J. Catal. 216 (2003) 477–486.
[39] M. Mogensen, P. Vang Hendriksen, in: S.C. Singhal, K. Kendall (Eds.), High Temperature Solid Oxide Fuel Cells: Fundamentals, Design and Applications, Elsevier, New York, 2003, pp. 261–289.